# Behaviour of stainless steel beam-to-column joints - Part 1: Experimental investigation

Elflah, Mohamed; Theofanous, Marios; Dirar, Samir; Yuan, Huanxin

Link to publication on Research at Birmingham portal

- The papers reports for the first time experimental results on full-scale stainless steel beam-to-column joints
- Stainless steel joints are shown to possess excellent ductility and high strength
- Current design standards are assessed and found overly conservative in the strength prediction of stainless steel joints
- Current design standards do not accurately predict the observed failure mode

# Behaviour of stainless steel beam-to-column joints - Part 1: Experimental investigation

**Mohamed Elflah[a], Marios Theofanous*[a], Samir Dirar[a], Huanxin Yuan[b]**

[a] *Department of Civil Engineering, University of Birmingham, Birmingham B15 2TT, United Kingdom*

[b] *School of Civil Engineering, Wuhan University, Wuhan 430072, PR China*

*corresponding author:

**Dr Marios Theofanous**, *Department of Civil Engineering, University of Birmingham, Birmingham B15 2TT, UK*

 Email: m.theofanous@bham.ac.uk

## Abstract

Research on stainless steel structures has primarily focused on the structural response of individual members, whilst the response of joints has received far less attention to date. This paper reports for the first time full-scale tests on stainless steel beam-to-column joints, subjected to static monotonic loads, whilst the companion paper reports numerical studies on similar connection typologies to the ones studied herein. The joint configurations tested include one flush and one extended end plate connection, two top and seated cleat connections, and two top, seated and web cleat connections of single-sided beam-to-column joints. All connected members and connecting parts including bolts, angle cleats and end plates are in Grade EN 1.4301 stainless steel. The full moment-rotation characteristics were recorded for each test and the experimentally derived stiffness and moment resistance for each joint was compared to the codified provisions of EN1993-1-8. It was verified that the connections displayed excellent ductility and attained loads much higher than the ones predicted by design standards for carbon steel joints.

## Keywords

Stainless steel joints, beam-to-column joints, Eurocode 3, Experimental tests, Semi-rigid connections


## 1     Introduction

The increasing importance of sustainability and a transition towards whole life costing has led to an increased interest in the use of stainless steel as a primary structural material [1-4]. The design of stainless steel structures has traditionally relied upon assumed analogies with carbon steel design thus not accounting for the actual material response which exhibits significant strain hardening and absence of a yield plateau. Thanks to numerous research efforts, several international standards covering the design of stainless steel structures were either recently published or revised recently [5-7] in line with the observed structural response for cross-sections in compression, bending [8] and shear [9].

Most published research on structural stainless steel design has focused on the behaviour of individual cross-sections and members, whilst the response of connections remains largely unverified. No significant difference between stainless steel and carbon steel joints is expected regarding the initial rotational stiffness, as the Young's modulus of both materials is similar and hence the geometric configuration will be determining the rotation stiffness. However, given that connections are subjected to localized high deformation demands in conjunction with the pronounced strain-hardening of stainless steel, carbon steel connection details commonly assumed pinned, may be able to transmit significant moments if they are employed in stainless steel. Moreover,

due to the higher material ductility of stainless steel, significant gains in terms of rotation capacity and hence overall ductility and resilience of the structure are expected, however they have not been quantified to date.

Some early experimental research on stainless steel bolted and welded connections was conducted by Errera et al [11], whilst more recently, the curling of bolted thin-walled stainless steel connections in shear was investigated by Kim et al [12, 13]. Ryan [14] reported tests on thick stainless steel bolted connections and Salih et al [15, 16] validated numerical models against the test reported in [14] and studied the net cross-section failure and the bearing failure of stainless steel bolted lap joints including austenitic, ferritic and duplex grades in their study. Moreover, they also studied numerically the behaviour of stainless gusset plate connections [17]. Bouchair et al [18] investigated numerically the response of stainless steel lap joints and t-stubs, whilst Cai and Young [19, 20] studied the response of stainless steel bolted joints at room and elevated temperatures.

Departing from studies on simple connections primarily transmitting shear forces, Tao et al [21] have recently published a paper on blind bolted connections of steel beams to concrete filled stainless steel columns where SHS and CHS concrete filled stainless steel sections were connected to a steel beam with or without a slab. Both monotonic and cyclic loading was considered. With the exception of this paper, no other study on full-scale stainless steel beam to column joints has been published to date. Moreover, [21] focuses on a composite joint configuration which does not facilitate the assessment of current design provisions for stainless steel joints [10], as the presence of concrete slab and the interaction of concrete infill and blind bolts complicate the response. An attempt to study numerically the response of top and seat cleat stainless steel beam-to-column joints was also recently reported by [22]. However, due to the absence of relevant test data, the validation of the numerical models was based on existing carbon steel experimental results, and assumptions regarding the material response and the interaction of the various stainless steel components in the numerical model were made.

This brief literature survey clearly highlights the need for full-scale tests on stainless steel beam-to-column joints. Experimental characterization of the behaviour of stainless steel joints will allow certain restrictions in EN 1993-1-4 [6] to be overcome, as for example plastic global analysis is currently not allowed in the absence of experimental evidence as "there should be evidence that the joints are capable of resisting the increase in internal moments and forces due to strain hardening ". To this end an experimental programme on structural response of stainless steel joints and joint components is underway. Six full scale tests on single-sided stainless steel beam-to-column joints are reported herein, whilst a comprehensive numerical study on stainless steel joints is reported in the companion paper [23]. Tests on stainless steel t-stubs under tension have been recently conducted and are reported in [24]. The tests will allow current design provisions of EN 1993-1-8 [10] to be assessed and particularly the provisions for plastic moment resistance, rotational stiffness available rotation capacity. It is envisaged that the reported experimental results will enable other researchers to conduct numerical studies on stainless steel joints based on FE models validated against relevant test data.

## 2 Experimental study

### 2.1 Details of tested specimens

All specimens employed a welded stainless steel section I 240×120×12×10 (i.e. outer depth h=240 mm, flange width b=120 mm, flange thickness $t_f$=12 mm, web thickness $t_w$=10 mm) for both the column and the beam. Four

joint types, commonly encountered in practice, have been considered. These include the extended end plate connection (EEP), the flush end plate connection (FEP), the top and seat angle cleat connections (TSAC) and the top, seat and double web cleat connection (TSWAC). Typically, equivalent carbon steel TSWAC and EEP connections are on the stiff side of the semi-rigid range depending on the connection geometry and material properties relative to the beam size and strength, whilst the TSAC and the FEP connections are usually closer to the flexible bound of the semi-rigid range [25]. As the focus of the paper lies in the response of the joint, the connections have been designed so that failure is confined in the connection region. Hence all joints were designed as partial strength joints and, due to their geometry, they were also semi-rigid.

Fig.1 shows the geometry of the four connection types considered. In all cases the bolts used are fully threaded M16 in Grade A4-80 (equivalent of 8.8 for carbon steel bolts) in 18 mm clearance holes. For the TSAC and the TSWAC connections the top and bottom angle cleat geometry is identical (including bolt hole locations) and two thicknesses for the angle cleats were considered to study the effect of angle cleat thickness on stiffness, strength and rotation capacity. It should be noted that the selection of the thickness for the end plates and the angle cleats was based on the maximum recommended thickness of an end plate or an angle cleat for which the connection may be assumed to possess sufficient rotation capacity according to Eq. (1) as given in EN 1993-1-8 [10].

$$t = 0.36d\sqrt{\frac{f_{u,b}}{f_y}}$$

(1)

In Eq. (1) the nominal bolt strength and the nominal yield stress of the angle cleats/end plates as stated in the mill certificates was used. The mill certificate values for the nominal yield stress (i.e. 0.2% proof stress) $\sigma_{0.2}$, the 1% proof stress $\sigma_{1.0}$, the ultimate tensile stress $\sigma_u$ and the strain at fracture $\varepsilon_f$ are summarized in Table 1. The resulting allowable thickness according to Eq. (1) was equal to 8.4 mm for the angle cleats and 8.9mm for the end plates.

## 2.2 Material properties

Flat coupons were extracted from the flange and the web of the I-section, from the angle cleats and from the same material from which the end plates were cut. The coupons were tested under strain control with an applied strain rate of 0.007%/s up to the 0.2% proof stress $\sigma_{0.2}$ and then a strain rate of 0.025%/s was applied until fracture in accordance with [26]. Fig.2 shows some representative stress strain curves for the material coupons extracted from the I-section and the angles. In addition to the material coupons, bolts from the same batch as the ones used for the specimens were tested in tension and in double shear to obtain the basic material response and facilitate the analysis of the experimental results. Figs.3 and 4 illustrate the load-deflection curves and failure modes of stainless steel bolts in double shear and in tension resepctively. Table 2 reports the key material properties obtained from the tensile tests. In all cases the proof stresses and ultimate tensile stresses reported in Table 2 are lower than the respective mill certificate values. This is attributed to possible differences in the orientation in which the coupons were tested, which coupled with stainless steels' anisotropy can have a significant effect on the obtained results. An additional reason for the observed discrepancy is the lower strain rate at which the material coupon tests were conducted in the lab compared to the strain rate used for the mill certificate tests. In the remainder of the paper and in the companion paper [23] the material properties reported

in Table 2 are used. The allowable end plate/angle cleat thickness based on Eq. (1) and the measured material properties is 9.7 mm.

## 2.3   Experimental setup and instrumentation

Fig. 5 illustrates the experimental setup and instrumentation employed in all tests. The length of the members and the support conditions were designed to allow a stress pattern representative of typical single-sided beam-to-column joints to develop in the joint, whilst ensuring that all deformations are confined in the joint and that failure occurs in either the beam or the column outside the joint region. All beams and columns were 1.5 m long. The column was inserted and wedged in a steel sleeve rigidly connected to the strong floor of the lab thereby facilitating fixed end conditions, as shown in Fig. 6. The horizontal displacement of the top of the column in the plane of the joint was restrained by a reaction frame. The load was applied vertically at 1.47 m from the column face via a hydraulic actuator, which was connected to the beam free end via a special bracket designed to eliminate any rotation of the beam end and hence any lateral torsional buckling of the beam, as shown in Fig. 6.

The employed instrumentation is partly shown in Fig.5. It consists of eleven LVDTs used to monitor displacements in key parts of the specimens, a load cell recording the horizontal reaction force exerted by the reaction frame to the top of the column, a load cell embedded in the actuator that records the applied force and strain gauges at key locations of the connections to monitor the evolution of strains and possible strain concentrations and localized plastic deformations, as shown in Fig. 7. The LVDTs, marked as L followed by a number in Fig. 5, were used to obtain the rotation of the beam $\Phi_b$ (independently computed from L1 -L2, L3-L4 and L3-L11), the rotation of the column $\Phi_c$ (L8-L9), possible separation of the end plate/angle cleat from the column face due to bolt elongation or bolt stripping (L5-L6) and to check that the employed details at the column ends (L7, L10) are stiff enough to restrain any displacement at the column ends. All instrumentation was connected to a data acquisition system and readings were recorded every two seconds.

## 2.4   Testing procedure

Prior to testing, the column of each specimen was inserted and wedged in the steel sleeve, as shown in Fig. 6. The beam was connected to the column with bolts, which were hand-tightened to obtain a snug tight connection, since preloaded bolts were beyond the scope of the project. Loading was applied via a hydraulic actuator with a maximum capacity of 400 kN and a maximum stroke travel of 250 mm. Upon connecting the LVDTs and strain gauges to the data acquisition system, the test commenced. The load was applied at a rate of 1.5mm/minute at the beam end. At regular intervals of about 10% of the expected ultimate load the test was halted for at least 2 minutes to obtain the quasi-static force. In practice, the test was halted for longer periods to allow the specimen to be photographed and to conduct some initial processing of the results and check that the specimens were behaving as expected. When large inelastic deformations developed and the failure seemed imminent the loading rate was decreased to 1 mm per minute and the test was halted more frequently. All specimens were tested to failure, which, as discussed later, was in all cases ultimately due to bolt failure in tension/bending or shear. From the tests conducted on the FEP and the TSWAC specimens, which were the first to be tested, it became apparent that the deformation of the joint between the attainment of the maximum load and the fracture of a bolt was insignificant, compared to the very large rotations corresponding to the maximum applied load.

Hence the remaining tests were terminated shortly after the maximum load was attained (i.e. the applied load started decreasing with increasing applied displacement). In those cases, inspection of the most heavily loaded bolts revealed crack initiation in the bolts.

# 3    Results

In this section, the obtained results are discussed in detail. Emphasis is placed on the observed failure modes and the overall moment rotation response, which are discussed separately for each type of joint hereafter. The moment acting on the joint was determined by multiplying the force applied by the actuator by the distance of the actuator from the column face (1.47 m), whilst the joint rotation $\Phi$ was determined by subtracting the rotation of the column $\Phi_c$ from the rotation of the beam $\Phi_b$. These rotation values were obtained from the relevant LVDT readings as previously mentioned. A typical moment-rotation curve is shown in Fig. 8, where the rotation is based on different LVDT readings. Very little difference can be observed between the beam rotation calculated by LVDTs L1-L2 and L3, L4 and L11, hence, only the beam rotation as determined by L1 and L2 is considered in the remainder of the paper.

## 3.1    Flush and extended end plate connections

Fig.9 depicts the obtained moment-rotation response for the FEP and EEP specimens. Both graphs exhibit an initial linear elastic response until about a third of the maximum recorded moment, whereupon a gradual loss of stiffness occurs followed by another almost linear region, as indicated by the smooth transition between the two lines. The second linear part of the response curves sharply once the maximum moment $M_{j,u}$ is reached. The FEP specimen exhibits a sharp linear post-ultimate response following the attainment of the maximum load which coincides with the failure of the bolt and is terminated upon the fracture of the bolt. This post-ultimate response was not recorded for the EEP specimen as the test was terminated shortly after the maximum load was reached. As expected, EEP is characterized by a stiffer response and a higher moment resistance, since the bolts beyond the top flange of the beam are more effective in transmitting the bending moment. However, FEP has markedly higher ductility with a rotation at ultimate load $\Phi_{j,u}$ more than 150 mrad, whilst the corresponding value for the EEP specimen is 119 mrad. The excellent ductility and the sharp increase in the moment resistance with increasing strain exhibited by both specimens is arguably partly attributable to material characteristics of stainless steel.

In Figs.10a and 10b the failure modes for FEP and EEP can be seen together with the most heavily stressed bolt for each specimen. In the case of the FEP, very large plastic deformations of the end plate can be observed, together with plastic bending of the column flange which is also clearly seen. The large deformations of the plate forced the heavily stressed top bolts of the connection to rotate leading to failure by fracture of one of the top bolts, whereupon the connection failed and the test was terminated. The fracture of the bolt occurred in the shank close to the bolt head, without any pronounced plastic deformation or necking, thus verifying that fracture of the bolt was primarily due to the forced rotation/flexure of the bolt head. In the case of the EEP specimen, a classical deformation of the t-stub comprising the beam tension flange and the end plate between the top and middle row of the bolts can be seen. The deformation of the t-stub corresponds to complete yielding of the flange between the bolt rows (Mode 1 according to [10]) and is known to be a ductile failure mode. Little deformation of the column flange in contact with the t-stub can be observed, whilst bearing of the beam

compression flange against the column flange has led to clear bending of the column flange in the compression zone. Failure was ultimately due to bolt failure, which can be seen in Fig.10b to have significant plastic deformations corresponding to tension and single shear as expected. A close inspection of the bolt revealed the initiation of tensile cracking, which triggered failure. It should be noted that in neither FEP or EEP specimens were any signs of weld fracture or fracture of the plate observed, thus verifying the excellent ductility of austenitic stainless steels.

In Fig. 11 the evolution of strains with increasing rotation are shown, with tensile strains being assigned a negative sign.). As expected, Fig. 11(a) shows high inelastic tensile strains in locations 1, 2, which lie the farthest from the joint's centre of rotation with decreasing tensile strains recorded in locations 4, 5 and 6 which lie closer to the centre of rotation and hence are subjected to smaller deformations. In accordance with the deformation pattern of the flush plate shown in Fig. 10(a), high inelastic compressive strains are observed in location 3. Similarly, Fig. 11(b) illustrates the evolution of very high tensile strains in locations 1 and 3 (between the top and the second bolt row) due to the pronounced bending of the end plate with decreasing tensile strains for locations 5 and 6 (between the second and the bottom bolt row). Compressive strains have been recorded in locations 2 and 4 which lie at the top and the second bolt row respectively.

## 3.2 Top and seat angle cleat connections

The moment-rotation response of the TSAC-8 and TSAC-10 specimens is shown in Fig.12. Both specimens exhibit similar response with an initial non-linear response attributable to the gaps between the bolts and the bolt holes followed by a linear elastic response leading to a gradual transition to a second, less stiff, linear region. For the thinner TSAC-8 specimen, the second linear region is followed by a nonlinear hardening region prior to failure. This is due to the change in shape of the top angle cleat, which with increasing deformation, transfers higher loads via tension rather than bending, hence displaying a stiffer response as it flattens. As expected, the thicker TSAC-10 specimen displays higher strength and stiffness compared to its thinner counterpart. In terms of ductility, both specimens reached similar values of rotation $\Phi_{j,u}$ corresponding to the maximum recorded load $M_{j,u}$ in excess of 150 mrad.

Fig.13 shows the observed failure modes, which include plastic deformation of the top cleat in the tension zone, limited plastic bending of the seat cleat in the compression zone and significant bending of the column flange in the compression zone due to bearing of the compression flange of the beam. As in the case of EEP and FEP, failure of the joint was ultimately triggered by bolt failure, which exhibited high inelastic deformations in shear and tension. In Fig.13, a hairline crack at the location of the shearing plane can be observed.

Fig.14 shows the evolution of strains in the top angle cleat connecting the top flange of the beam to the column face for specimens TSAC-8 and TSAC-10 with increasing rotation. The compressive strains are assigned a positive sign and the tensile strains a negative one. The strains between the two bolt holes of the horizontal leg of the angle cleat connecting it to the beam's top flange (location 1) remain fairly small throughout the loading process, as that part of the angle cleat does not deform significantly. As expected, high tensile strains develop in the vicinity of the toes of the angle legs as the angle cleats deform in an opening mode with increasing rotation.

The strains in the horizontal leg of the cleat (beam side - location 2) increase faster than the strains in the vertical leg (column side - location 3) and the two curves diverge increasingly with increasing deformation. This is more pronounced for the thinner angle cleat (Fig. 14 (a)), which displays higher plastic deformation, whilst for the thicker angle cleat (Fig.14 (b)) the curves for locations 2 and 3 diverge less. Finally, high compressive strains can be observed between the bolt holes in the vertical leg of the angle cleat (location 4) due to the localized bending of the angle cleat. Overall the recorded strains are in good agreement with the observed deformation.

### 3.3 Top, seat and web cleat connections

Fig.15 shows illustrates the recorded moment-rotation for the TSWAC-8 and TSWAC-10 joints. The response of both specimens is similar and exhibits the initial non-linear part of reduced stiffness due to lack of contact between the bolts and the clearance holes as discussed before. As expected, the TSWAC specimens are stiffer and stronger than their counterparts without the web cleats. Regarding the effect of the employed angle cleat thickness, there seems to be a marked effect on the initial stiffness and the rotation at maximum moment $\Phi_{j,u}$, however the maximum moment itself remains unaffected, as is the stiffness of the second linear branch of the moment-rotation curve.

Failure of both specimens occurred due to failure of the top bolt connecting the web cleat to the beam in double shear, as can be clearly seen in Fig.16, where the failed bolt can be clearly seen to exhibit plastic shear deformations and the two slip planes in the bolt shank are clearly visible. Some plastic bending of the column flange due to bearing of the beam compression flange on the column can also be observed, this however occurred at very high rotation values. Fig.17 illustrates the evolution of strains in the top and web angle cleats connecting the top flange and the web of the beam respectively to the column face for specimens TSWAC-8 and TSWAC-10. The strain evolution in the top angle cleat follows closely the trends observed in Fig.14 for the TSAC specimens, with high inelastic strains being present in the vicinity of the angle toe and in the vicinity of the bolt holes of the vertical angle cleat leg (locations 2, 3 and 4). High inelastic strains develop in the web cleat toe on the beam side (location 6), thus indicating the concentration of high plastic deformations in this region. The development of strains in location 6 overall follow the evolution of strains in locations 2 and 3 but are slightly lower, since location 6 is closer to the centre of rotation of the joint than locations 2 and 3, hence the imposed deformation due to the joint rotation is smaller. Significant strains develop in the leg of the web cleat on the column side of TSWAC-8 specimen (Fig. 17 (a)), which, as shown in Fig. 16(a), deforms with increasing rotation. For the thicker TSWAC-10 specimen (Fig. 17(b)) virtually no strain is seen to develop in location 7. Similar to location 1, very low strains can be observed in location 5.

### 3.4 Key joint response characteristics

Several useful parameters relating to strength, stiffness and rotation capacity were extracted from the graphs and are summarized in Table 3, to allow the recorded response to be characterized and compared to the one predicted by EN 1993-1-8 [10]. These include the initial stiffness $S_{j,ini}$ , the pseudo plastic moment resistance $M_{j,R}$ and its corresponding rotation $\Phi_{j,R}$, the maximum obtained moment $M_{j,u}$ its corresponding rotation $\Phi_{j,u}$ and

the maximum recorded rotation $\Phi_c$, which are obtained from the moment rotation curves. All symbols are defined in Fig. 18.

The initial stiffness $S_{j,ini}$ was obtained by regression analysis of the initial linear part of the curve prior to the development of any plastic deformations. For specimens FEP, EEP, TSAC-8 and TSAC-10, where the initial linear part is preceded by a nonlinear region due to the existence of gaps between the bolts and the clearance holes, the initial linear part is ignored and the regression analysis is carried out over the part of the curve which exhibits linear response. Similarly, the maximum moment $M_{j,u}$, the corresponding rotation $\Phi_{j,u}$ and the maximum recorded rotation $\Phi_c$ were also unambiguously determined. With respect to the pseudo plastic moment resistance $M_{j,R}$ which will be later on compared to the Eurocode moment resistance predictions there are several procedures according to which it can be determined from an experimental moment-rotation curve. These include the intersection between the second less stiff linear region of the curve with the vertical axis of the moment rotation curve [27], the moment value corresponding to the intersection between the lines tangent to the first (i.e. elastic) linear part of the curve and the second (i.e. hardening) linear part of the curve [28] and the moment value of the curve at a secant stiffness defined as a fraction of the initial elastic stiffness [29]. The first procedure has the advantage of being independent of any initial nonlinear response of the moment-rotation curve, the second one is similar but less conservative than the first and the third one has been adopted by EN1993-1-8 [10], but relies on the accurate prediction of the joint stiffness, which can display significant scatter for bolted connections due to gaps between the bolts and their clearance holes. All three procedures are schematically shown in Fig.18. In this and the companion paper [23], the $M_{j,R}$ values are determined from the intersection between the initial elastic stiffness and the  line tangent to the hardening part of the curve as outlined in [28], since this procedure has been widely adopted by researchers [30, 31]. The obtained values for $M_{j,R}$ are reported in Table 3 and are used hereafter to assess the accuracy of the design equations of EN 1993-1-8 [10]. Finally, the value of the moment corresponding to a rotation of 30 mrad, which is widely considered as a sufficient rotation capacity for beam-to-column joints [30-32] has also been included in Table 3. It should be noted that the value of 30 mrad is inbetween the minimum required values for the rotation capacity of a plastic hinge specified for steel dissipative connections in [33] as 35 mrad and 25 mrad for ductility class high (DCH) and ductility class medium (DCM) respectively.

## 4    Discussion

Having obtained the basic characteristics of the response of the tested joints, the predictions of EN 1993-1-8 [10] for carbon steel joints with respect to the initial rotational stiffness, strength and ductility are hereafter compared to the experimental ones.

### 4.1    Initial rotational stiffness

The initial rotational stiffness $S_{j,ini}$ of the tested joints is calculated from Eq. (2) according to the provisions of EN 1993-1-8 [10]:

$$S_{j.ini} = \frac{Ez^2}{\sum_i \frac{1}{k_i}}$$

(2)

where E is the Young's modulus, z is the leverarm and $k_i$ are the stiffness coefficients of the basic joint components considered for each connection.

In addition to the column web in tension and compression, the column flange in bending and the bolts in tension, which are considered for all joints, the end plate in bending is considered for the FEP and EEP joints, the angle cleats in bending and bearing and beam flanges and beam web in bearing and the bolts in shear are considered for the TSAC joints and TSWAC specimens. The measured values for Young's modulus were used for each component considered, whilst the $k_i$ values are determined according to EN 1993-1-8 [10]. For the determination of the stiffness of the FEP, EEP and TSAC joints, [10] gives specific provisions relating to the determination of z and, whilst the determination of the stiffness of TSWAC joints is not fully covered. Therefore, design recommendations for the strength and stiffness of TSWAC joints proposed in [34], which are essentially an extension of the component method of [10] have been employed herein.

The predicted values for the initial stiffness of the tested connections are summarized in Table 4 where the ratio of the predicted stiffness values over the experimental ones is also reported. On average, the EN 1993-1-8 [10] procedure overestimates the initial rotational stiffness by 94%. Similar conclusions were also reached for carbon steel end plate joints [30, 31], where the predicted stiffness was on average more than twice the experimental one, and for carbon steel TSAC and TSWAC specimens where a large scatter of the predictions has been reported [35, 36]. Hence the apparent inaccuracies of the design provisions for the rotational stiffness in [10] do not relate to a specific material, but are arguably attributable to the gaps and slips between the various bolted components of non-preloaded bolted connections, which cannot be easily quantified and are not taken into account in design standards.

## 4.2 Plastic moment resistance

The plastic moment resistance of all tested connections is obtained according EN 1993-1-8 [10], using the measured $\sigma_{0.2}$ values in place of the yield strength for the relevant components. The predicted plastic moment resistance $M_{j,R}$ is reported in Table 4 where the ratio of predicted over experimental plastic moment resistance is also reported. As expected, all Eurocode predictions are conservative with an average value of predicted over experimental moment resistance of 0.53 and a coefficient of variation 0.13. This indicates that the Eurocode consistently underestimates the capacity of stainless steel connections, at least for the six joints tested in this study. High levels of conservatism were exhibited by the Eurocode for other stainless steel components with much simpler structural behaviour, such as the moment resistance of restrained beams [8] and relate to the pronounced strain-hardening exhibited by stainless steel.

### 4.3 Rotation capacity and failure modes

The rotation capacity of steel connections is not quantified in [10]. Instead, simple design provisions are given, which, if followed, allow the designer to assume that the joint possess adequate rotation capacity. These include fulfilment of Eq.(1) and ensuring that the design moment resistance $M_{j,R}$ is governed by a ductile failure mode [36], such as column web panel in shear, column flange in bending or beam end plate or tension flange cleat in bending. As earlier discussed, how much rotation capacity is considered adequate depends on the application, with the European seismic design code specifying 25 mrad and 35 mrad as the minimum required connection rotations for DCH and DCM respectively. All joints tested in this study fulfilled the conditions specified in [10], and were thus expected to develop adequate rotation capacity, which is seen to be the case with recorded rotations ranging from 91 mrad to 165 mrad.

Table 5 reports the predicted failure modes according to [10], the observed failure modes at ultimate load, the recorded maximum rotation and the ratio of the experimentally derived ultimate moment over the experimentally determined plastic moment of the joint. The predicted failure modes are all ductile and include bending of the plate or angle cleats. However, as earlier discussed, in all cases failure was triggered by bolt failure either in tension or in shear. It should be noted that the predicted failure modes relate to the minimum strength of the weakest component at the attainment of the plastic moment resistance of the connection $M_{j,R}$, whilst the experimental failure modes, relate to the failure of a component when the maximum recorded moment $M_{j,max}$ was reached. The predicted failure modes according to [10] did indeed develop but the connections possessed significant overstrength and reached higher moments due to the excellent ductility and pronounced strain-hardening of the stainless steel plates and angle cleats, until the less ductile bolts failed. The $M_{j,max}$ over $M_{j,R}$ ratio, which can be considered an additional measure of ductility, ranges between 1.36 and 2.83. Both the minimum $M_{j,max}$ over $M_{j,R}$ ratio and the minimum joint rotation occur for the TSWAC10 specimen, the ultimate failure of which was due to shearing of the top bolt connecting the web cleats to the beam web.

## 5    Conclusions

Both this and the companion paper address the issue of very limited research on stainless steel joints, the design provisions for which are based on assumed analogies with carbon steel joints. Six full-scale tests on single sided beam to column joints made of austenitic stainless steel has been conducted and reported in detail. The tested joints included FEP, EEP, TSAC and TSWAC joints and exhibited high rotation capacity and overstrength due to the excellent ductility and pronounced strain-hardening of stainless steel. In all cases, significant inelastic deformations occurred in the end plates or angle cleats prior to failure which was ultimately due to bolt failure either in tension or in shear. Based on these limited experimental results, the provisions of EN1993-1-8[10] which are also assumed to be applicable to stainless steel joints have been assessed. Similar to studies on carbon steel joints, the stiffness model of the Eurocode was found to overestimate the initial rotation stiffness of the joints and the predictions displayed significant scatter. On the other hand, the strength predictions were found to systematically underestimate the plastic moment resistance of the tested joints. An important observation relates to failure always being triggered by bolt failure even in cases where according to EN 1993-1-8 [10] failure of the T-stub due to the formation of plastic hinges was expected. The T-stub did indeed develop the predicted

plastic deformation, but due to the significant strain-hardening of stainless steel, the stresses in the yielded regions and hence the moment resistance of the connection kept increasing until the less ductile bolts failed in tension as clearly exhibited in Figs 10 and 13. Hence, basing the prediction of the failure mode on the EN 1993-1-8 [10] design equations should be done with caution as failure to account for strain-hardening of the T-stubs results in the bolts potentially being subjected to much higher tensile forces than anticipated. Based on the six tests reported herein, numerical models for FEP, EEP, TSAC and TSWAC joints are developed and validated in the companion paper [23], and detailed parametric studies are conducted to allow a more comprehensive assessment of the provisions on EN 1993-1-8 [10].

## Acknowledgements

## References

[1] Rossi B. Discussion on the use of stainless steel in constructions in view of sustainability. Thin-Walled Structures 83: 182-189, 2014.

[2] Gedge G. Structural uses of stainless steel—buildings and civil engineering, Journal of constructional steel research 64(11): 1194-1198, 2008.

[3] Baddoo N.R. Stainless steel in construction: a review of research, applications, challenges and opportunities. Journal of Constructional Steel Research 64(11):1199-1206, 2008.

[4] Gardner L. The use of stainless steel in structures. Progress in Structural Engineering and Materials. 7(2):45-55, 2005.

[5] AISC 27, Design Guide 27 Structural Stainless Steel, American Institute of Steel Construction, 2013.

[6] EN 1993-1-4+A1, Eurocode 3: Design of steel structures - Part 1.4: General rules Supplementary rules for stainless steel, CEN, 2015.

[7] SEI/ASCE, Specification for the design of cold-formed stainless steel structural members, SEI/ASCE 8-02, Reston, VA, 2002.

[8] Gardner L., Theofanous M. Discrete and continuous treatment of local buckling in stainless steel elements, Journal of Constructional Steel Research 64(11):1207-1216, 2008.

[9] Saliba N., Real E., Gardner L. Shear design recommendations for stainless steel plate girders, Engineering Structures, 59: 220-228: 2014.

[10] EN 1993-1-8. Eurocode 3: Design of steel structures – Part 1-8: Design of joints., British Standards Institution, CEN, 2005.

[11] Errera S.J., Popowich D.W., Winter G. Bolted and welded stainless steel connections. Journal of Structural Engineering, ASCE 100(6): 2549-2567, 1974.

[12] Kim T.S., Kuwamura H. Finite element modeling of bolted connections in thin-walled stainless steel plates under static shear, Thin-Walled Structures, 45(4), pp. 407-421, 2007

[13] Kim T.S., Kuwamura H., Cho T.J. A parametric study on ultimate strength of single shear connections with curling. Thin-Walled Structures 46(1): 38-53, 2008.

[14] Ryan I. Development of the use of stainless steel in construction WP 4.2 ECSC Project No. 7210-SA/327, 1999.

[15] Salih E.H, Gardner L., Nethercot D.A. Numerical investigation of net section failure in stainless steel bolted connections, Journal of Constructional Steel Research 66(12):1455-1466, 2010.

[16] Salih E.H, Gardner L., Nethercot D.A. Bearing failure in stainless steel bolted connections, Engineering Structures 33(2):549-562, 2011.

[17] Salih E.H, Gardner L., Nethercot D.A. Numerical study of stainless steel gusset plate connections. Engineering Structures 49:448-464, 2013.

[18] Bouchaïr A., Averseng J., Abidelah A. Analysis of the behaviour of stainless steel bolted connections. Journal of Constructional Steel Research 64 (11):1264–1274, 2008.

[19] Cai Y., Young, B. Structural behavior of cold-formed stainless steel bolted connections, Thin-Walled Structures 83: 147-156, 2014

[20] Y. Cai, B. Young, Behavior of cold-formed stainless steel single shear bolted connections at elevated temperatures, Thin-Walled Structures 75: 63-75, 2014.

[21] Tao Z., Hasan M.K., Song T.-Y., Han L.-H. Experimental study on blind bolted connections to concrete-filled stainless steel columns. Journal of Constructional Steel Research 128:825-838.

[22] Hasan M.J., Ashraf M. Uy B. Moment-rotation behaviour of top-seat angle bolted connections produced

from austenitic stainless steel. Journal of Constructional Steel Research 136:149-161, 2017.

[23] Elflah M., Theofanous M., Dirar S. Behaviour of stainless steel beam-to-column joints - Part 2: numerical modelling and parametric study. (submitted 5th Itnernational stainless steel experts seminar/JCSR special issue on stainless stele structures)

[24] H.X. Yuan, S. Hu, X.X. Du, L. Yang, X.Y. Cheng, Theofanous M. Experimental behaviour of stainless steel bolted t-stub connections under monotonic loading. (submitted 5th Itnernational stainless steel experts seminar/JCSR special issue on stainless stele structures)

[25] Kishi N., Hasan R., Chen W.F., Goto Y. Study of Eurocode 3 steel connection classification. Engineering Structures 19(9): 772-779, 1997.

[26] BS EN ISO 6892-1:2009. British standard: metallic materials - tensile testing. Part 1: Method of test at ambient temperature. The Standards Policy and Strategy Committee; 2009.

[27] Jaspart J.P. Study of the semi-rigidity of beam-to-column joints and its influence on the resistance and stability of steel buildings, PhD thesis, Liège University, 1991.

[28] Zanon P., Zandonini R. Experimental analysis of end plate connections. Proceedings of the state of the art workshop on connections and the behaviour of strength and design of steel structures, Cachan:41-51, 1988.

[29] Weynand K. Sicherheits- und Wirtschaftlichkeitsuntersuchungen zur Anwendung nachgiebiger Anschlüsse im Stahlbau. Heft 35, Shaker Verlag, Aachen, 1997.

[30] Girão Coelho A.M., Bijlaard F.S.K., Simões da Silva L. Experimental assessment of the ductility of extended end plate connections. Engineering Structures 26:1185-1206, 2004.

[31] Girão Coelho A.M., Bijlaard F.S.K. Experimental behaviour of high strength steel end plate connections. Journal of Constructional Steel Research 63: 1228-1240, 2007.

[32] Wilkinson S., Hurdman G. Crowther A. A moment resisting connection for earthquake resistant structures. Journal of Constructional Steel Research 62: 295–302, 2006.

[33] EN 1998-1. Eurocode 8: Design of structures for earthquake resistance - Part 1: General rules, seismic actions and rules for buildings. British Standards Institution, CEN, 2004.

[34] Pucinotti R. Top-and-seat and web angle connections: prediction via mechanical model. Journal of constructional steel research 57(6): 661-694, 2001.

[35] KongZ., Kim S.E. Moment-rotation behavior of top-and seat-angle connections with double web angles. Journal of Constructional Steel Research 128: 428–439, 2017.
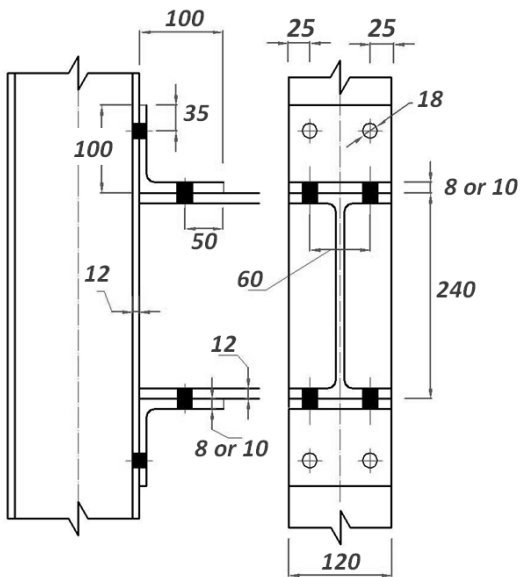
[36] Simões da Silva L., Santiago A., Vila Real P. Post-limit stiffness and ductility of end-plate beam-to-column steel joint. Computers & Structures 80(5-6): 515-531, 2002.
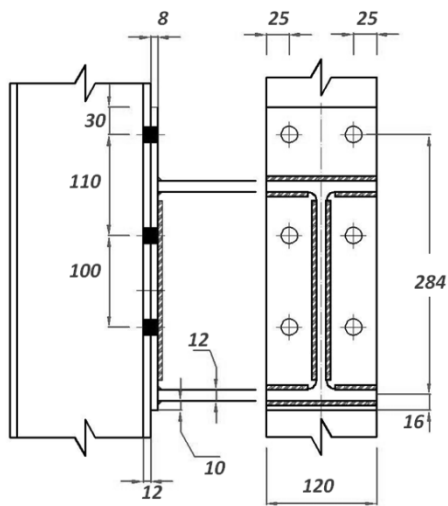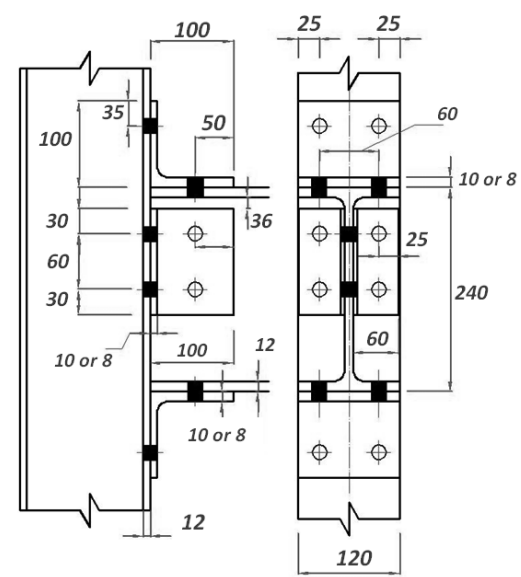
(a) Extended End Plate (EEP) connection
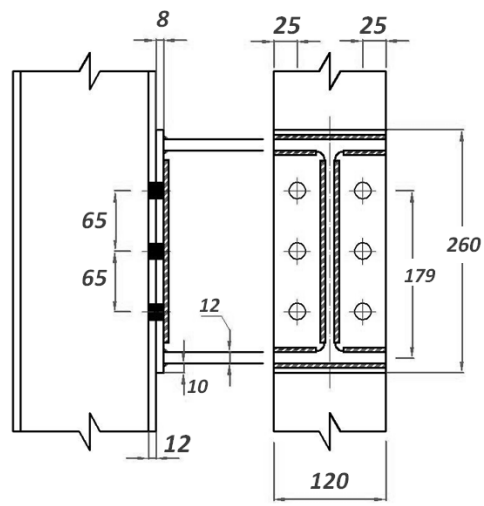
(b) Flush End Plate (FEP) connection

(c) Top and Seat Angle Cleat connection (TSAC)

(d) Top, Seat and double Web Cleat (TSWAC) connection

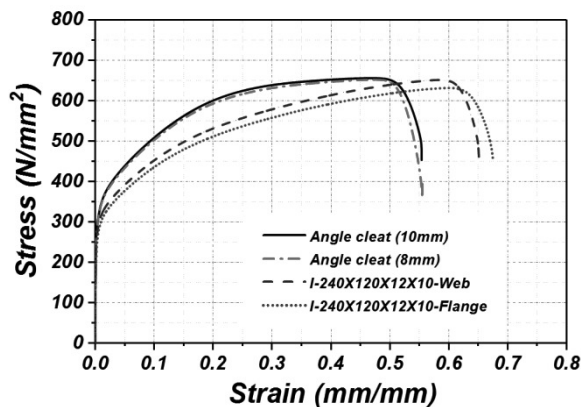Fig. 1    Geometric configuration of the tested specimens
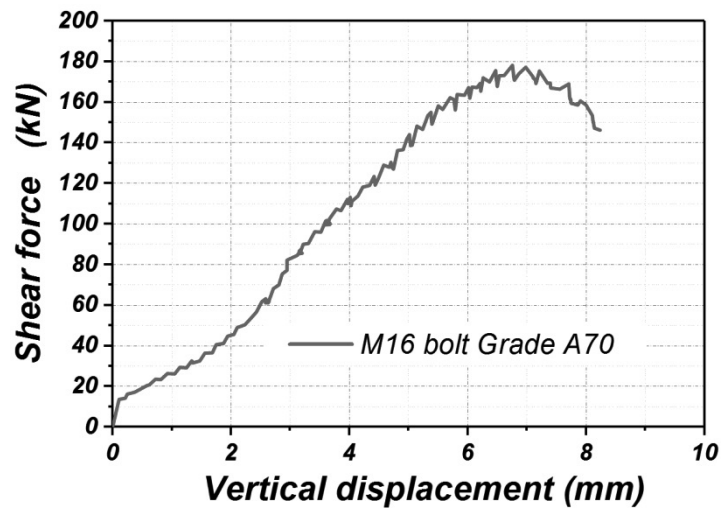


Fig.2 Typical stress strain curves of tested stainless steel tensile coupons.

**Fig.3 Load-deflection curve and failure mode of M16 bolt Grade A4-80 loaded in double shear.**
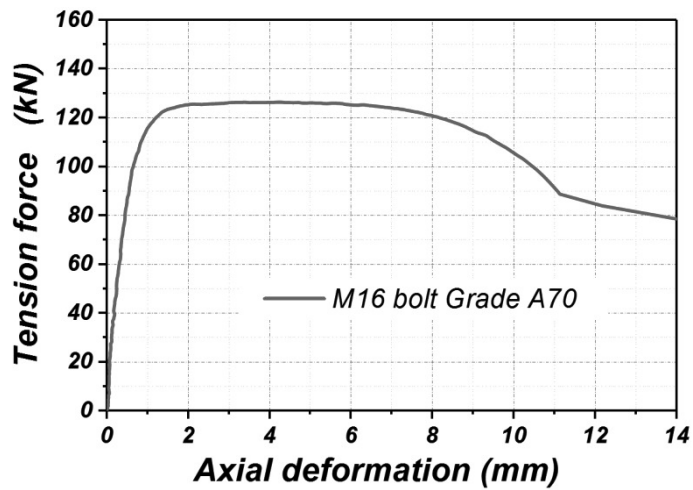


**Fig.4 Load-elongation curve and failure mode of M16 bolt Grade A4-80 loaded in tension.**
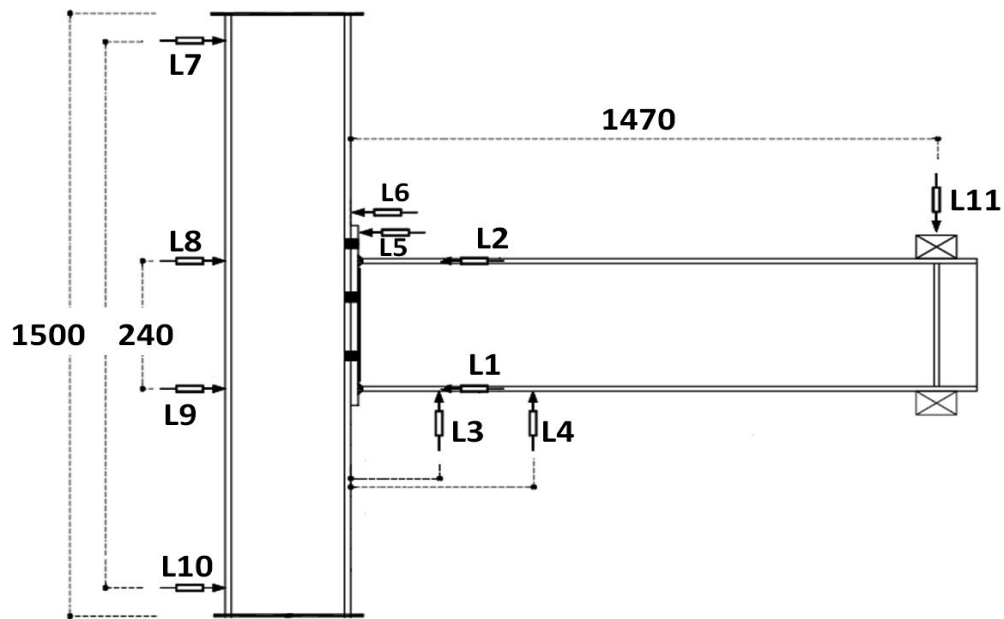
**Fig.5 General arrangement of experimental setup and instrumentation.**
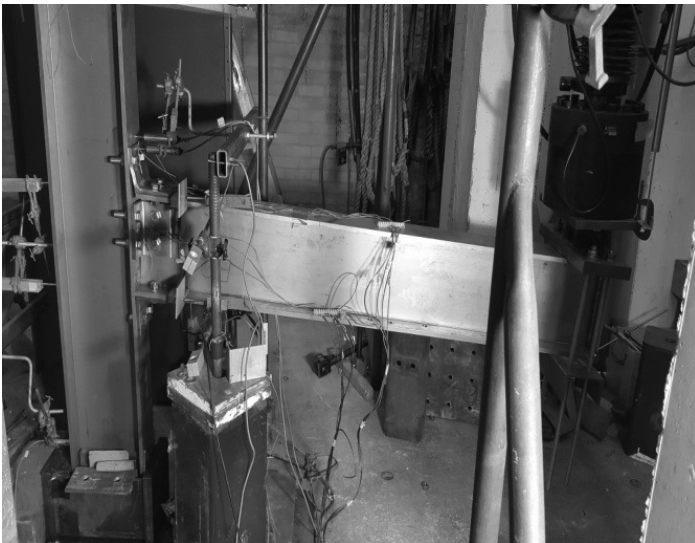


**Fig.6 Experimental setup during testing of TSWAC-8**
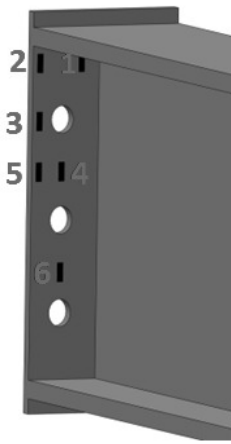
(a) FEP
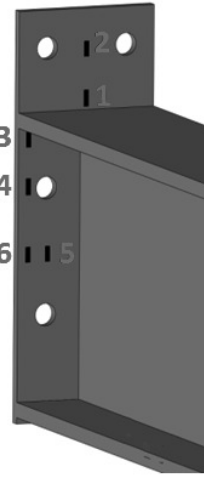
(b) EEP
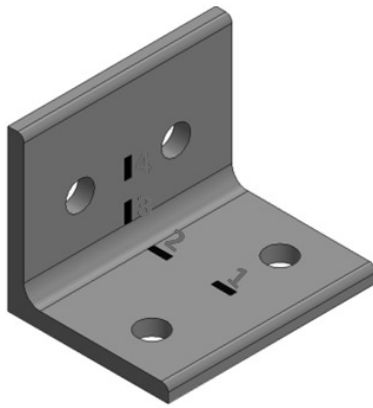
(c) TSAC-10 & TSAC-8
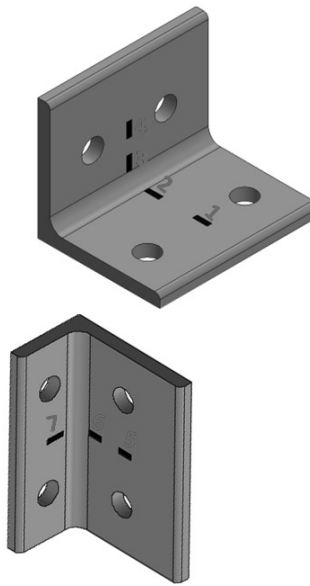
(d) TSWAC-10 & TSWAC-8

Fig.7 Location of strain gauges for each specimen
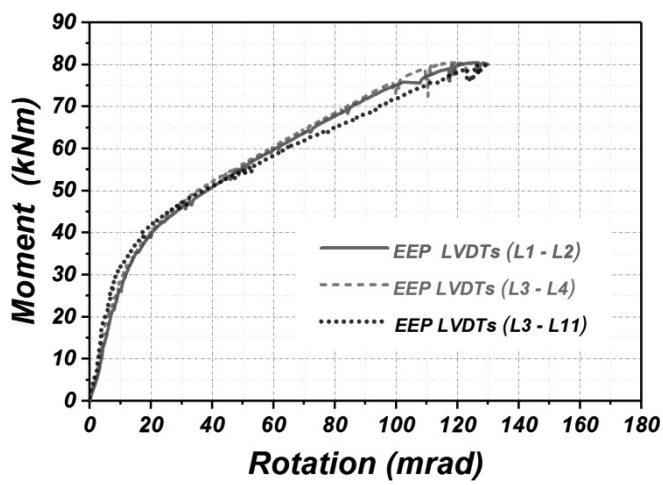


Fig.8 Moment rotation curves of EEP with different definitions of beam rotation $\Phi_b$
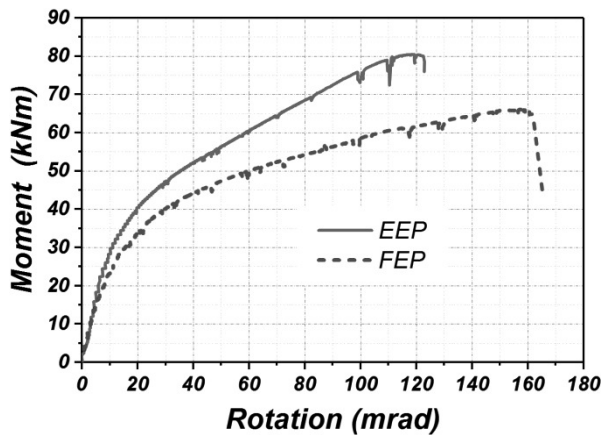
**Fig.9 Moment-rotation response for FEP and EEP specimens**
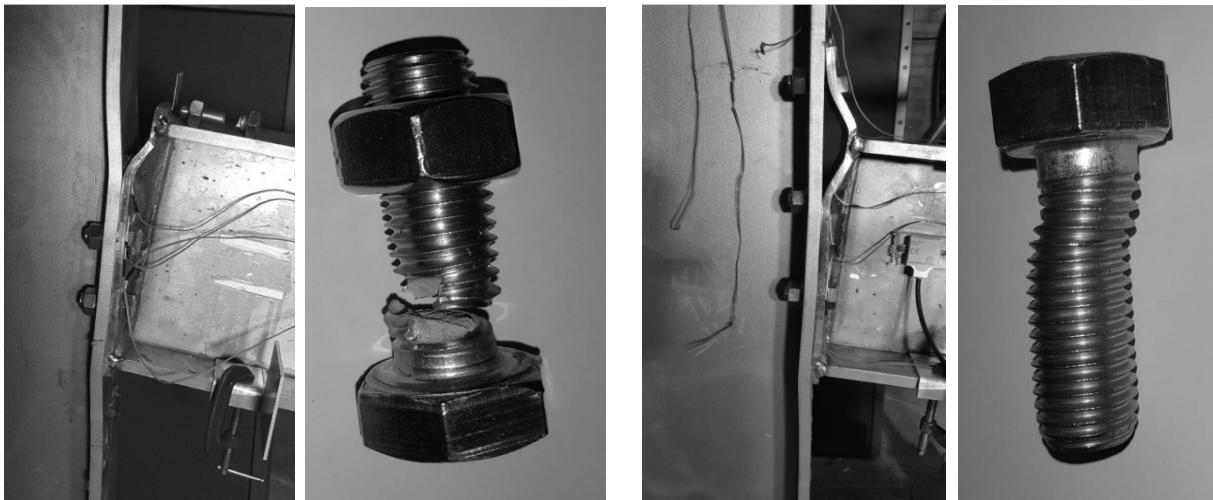


(a) Flush End Plate (FEP) connection failure mode and fractured top bolt

(b) Extended End Plate (EEP) connection failure mode and deformed top bolt

**Fig.10 Failure modes of FEP and EEP specimens**
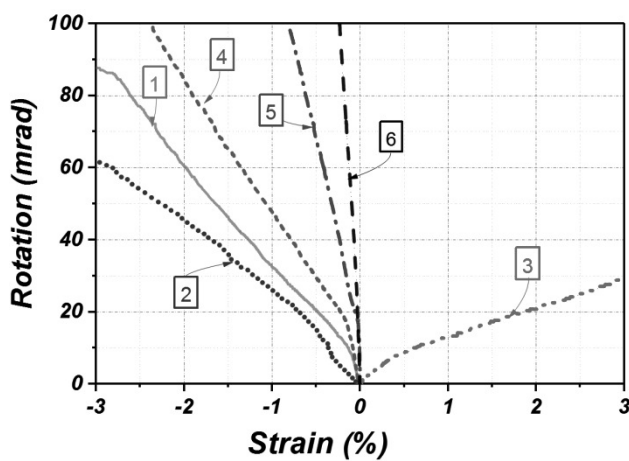


(a) Measured strains for FEP specimen
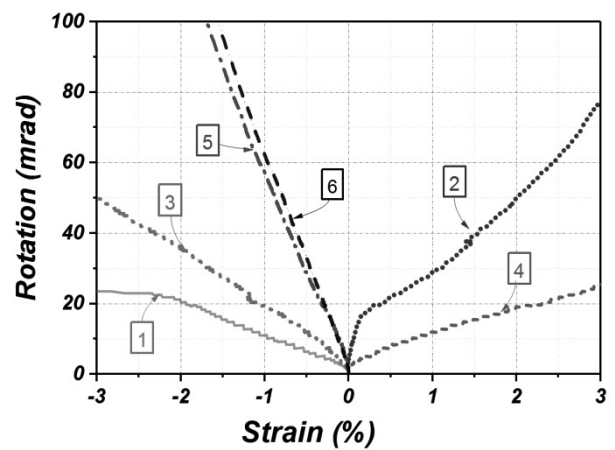
(b) Measured strains for EEP specimen

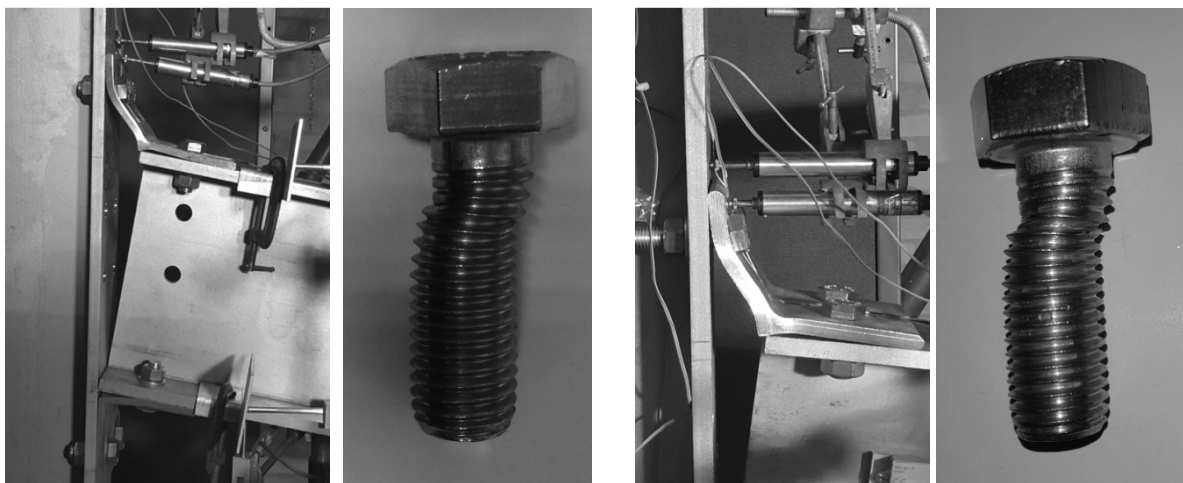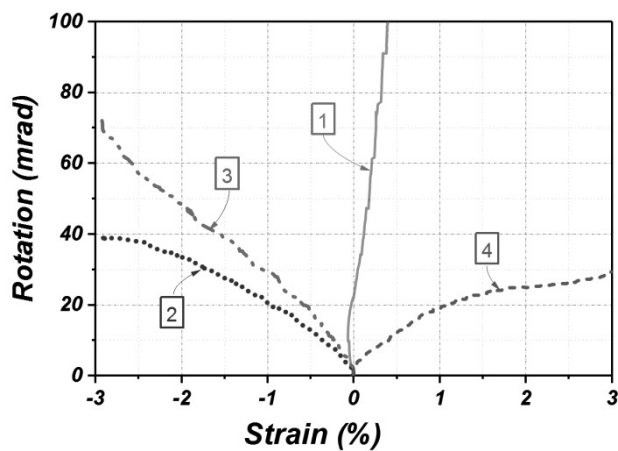**Fig.11 Strain evolution with increasing rotation for FEP and EEP specimens**
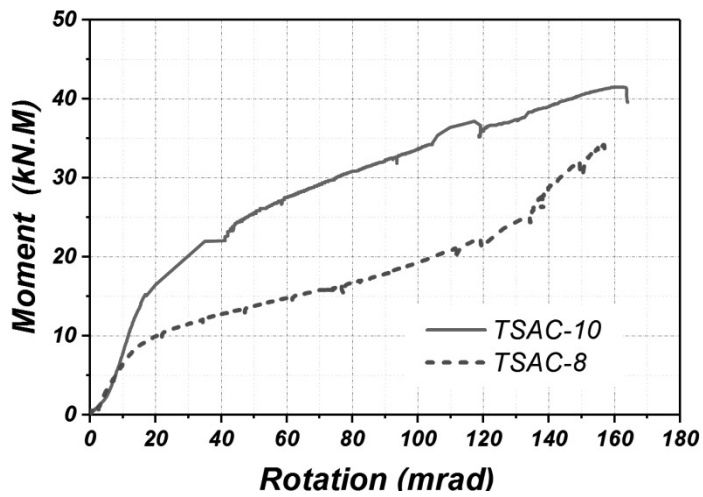
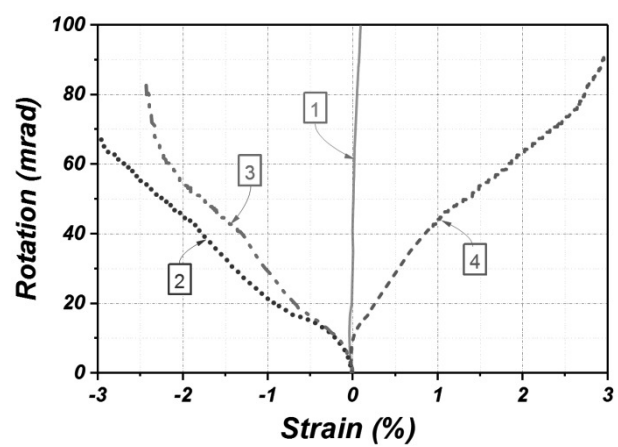**Fig.12 Moment-rotation response for TSAC-8 and TSAC-10 specimens**



(a) TSAC-8 connection failure mode and deformed top bolt

(b) TSAC-10 connection failure mode and deformed top bolt with crack initiation

**Fig.13 Failure modes of TSAC-8 and TSAC-10 specimens**



(a) Measured strains for TSAC-8 specimen

(b) Measured strains for TSAC-10 specimen

**Fig.14 Strain evolution with increasing rotation for TSAC-8 and TSAC-10 specimens**
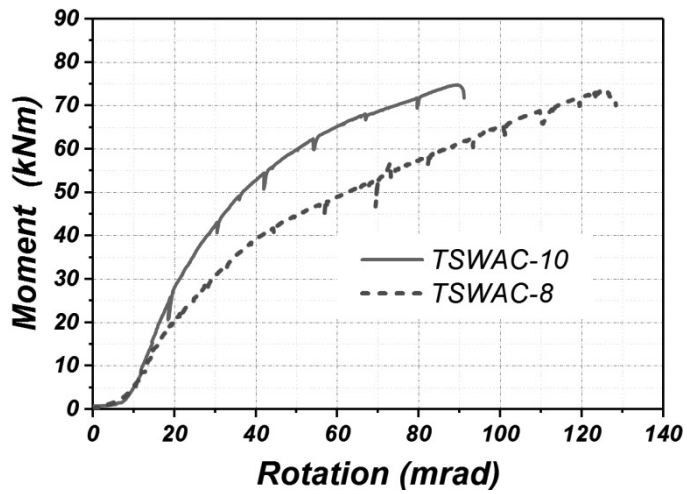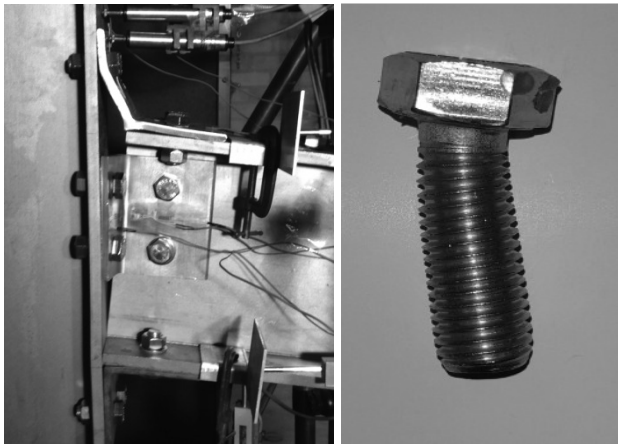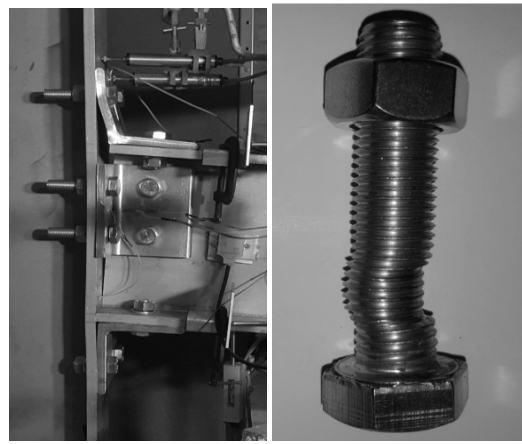
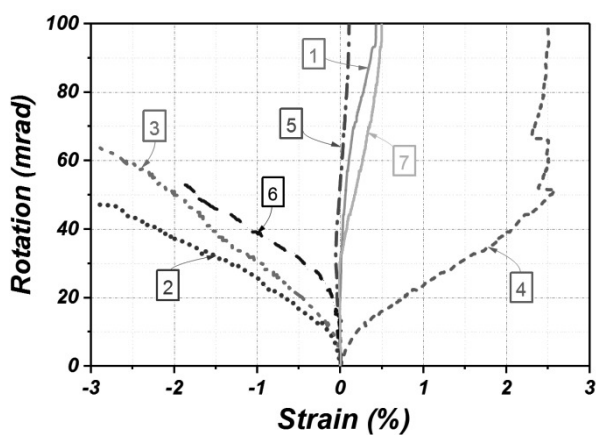Fig.15 Moment-rotation response for TSWAC-8 and TSWAC-10 specimens



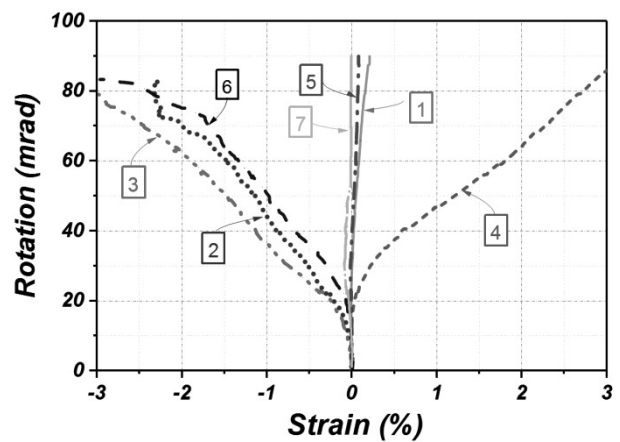(a) TSWAC-8 connection failure mode and deformed top bolt

(b) TSWAC-10 connection failure mode and deformed bolt in beam web failed in double shear

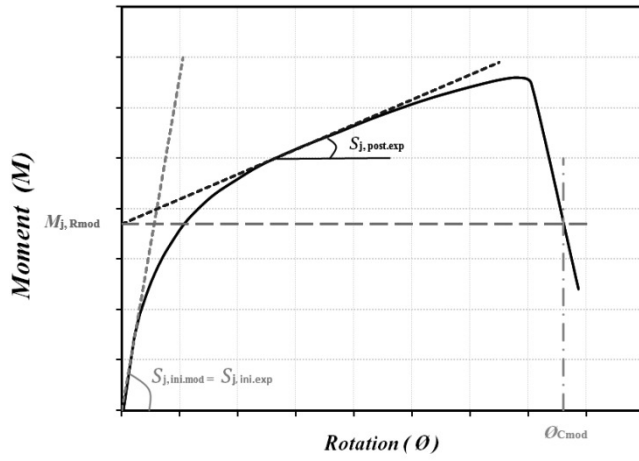Fig.16 Failure modes of TSWAC-8 and TSWAC-10 specimens



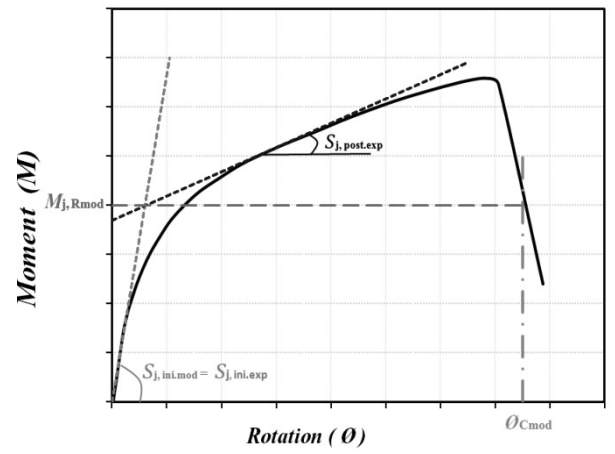(a) Measured strain for TSWAC-8 specimen
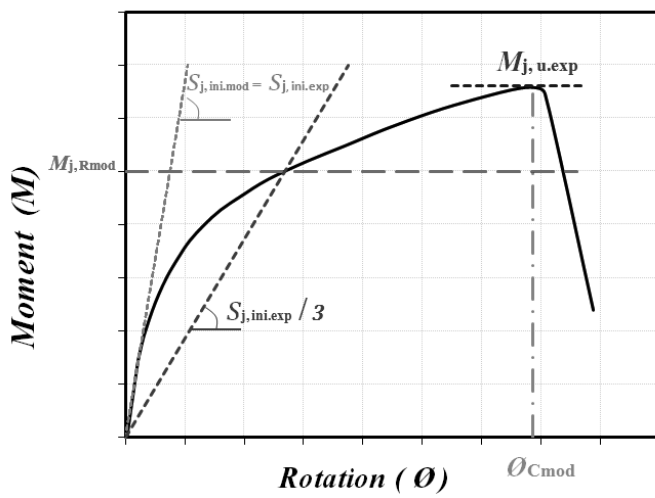
(b) Measured strain for TSWAC-10 specimen

Fig.17 Strain evolution with increasing rotation for TSWAC-8 and TSWAC-10 specimens

a) After Jaspart [27]



b) After Zenon and Zandonini [28]



c) After Weynard [29, 10]

Fig.18 Various definitions of plastic moment resistance

**Table 1  Material properties according to mill certificates**

| Specimen | $\sigma_{0.2}$ $(N/mm^2)$ | $\sigma_{1.0}$ $(N/mm^2)$ | $\sigma_u$ $(N/mm^2)$ | $\varepsilon_f$ % |
|---|---|---|---|---|
| I-240×120×12×10 | 341 | 369 | 635 | 53 |
| L-100X100X8 | 373 | 441 | 675 | 54 |
| L-100X100X10 | 378 | 445 | 673 | 55 |
| Endplate (thickness 8mm) | 335 | 379 | 630 | 54 |

**Table 2  Material properties from tensile tests**

| Specimen | E $(N/mm^2)$ | $\sigma_{0.2}$ $(N/mm^2)$ | $\sigma_{1.0}$ $(N/mm^2)$ | $\sigma_u$ $(N/mm^2$ | $\varepsilon_f$ % |
|---|---|---|---|---|---|
| I-240×120×12×10 - flange | 196 500 | 248 | 306 | 630 | 66 |
| I-240×120×12×10 - web | 205 700 | 263 | 320 | 651 | 65 |
| Angle cleat (8 mm) | 197 600 | 280 | 344 | 654 | 55 |
| Angle cleat (10 mm) | 192 800 | 289 | 353.5 | 656 | 56 |
| End plate | 198 000 | 282 | 343 | 655 | 54 |
| M16 bolt (A4-80) | 191 500 | 617 | 703 | 805 | 12 |

**Table 3  Key experimental results from the moment-rotation curves.**

| Specimen | Initial stiffness $S_{j,ini}$ (kNm/rad) | Maximum moment $M_{j,max}$ (kNm) | Moment at 30 mrad $M_{j,30}$ (kNm) | Plastic Moment resistance $M_{j,R}$ (kNm) | Rotation $\Phi$ (mrad) at maximum moment $\Phi_{j,u}$ | maximum recorded $\Phi_c$ |
|---|---|---|---|---|---|---|
| FEP | 3913 | 65,40 | 41 | 40 | 157 | 165 |
| EEP | 4464 | 80.40 | 48 | 42 | 119 | 121 |
| TSAC-8 | 1237 | 34.10 | 12 | 12 | 157 | 157 |
| TSAC-10 | 1521 | 41.50 | 21 | 23 | 162 | 162 |
| TSWAC-8 | 1920 | 73.30 | 30 | 39 | 125 | 131 |
| TSWAC-10 | 2769 | 74.70 | 44 | 55 | 91 | 95 |

**Table 4 Comparison of experimental results with EC3 predictions**

| Specimen | Initial stiffness $S_{j,ini}$ (kNm/mrad) | | | Moment Capacity $M_j$ (kNm) | | |
|---|---|---|---|---|---|---|
| | $S_{j,ini,}$ (EC3) | $S_{j,ini}$ (TEST) | EC3/Test | $M_{j,R}$ (EC3) | $M_{j,R}$ (TEST) | EC3/Test |
| FEP | 5740 | 3913 | 1.47 | 18.6 | 40 | 0.47 |
| EEP | 9360 | 4464 | 2.10 | 27.2 | 42 | 0.65 |
| TSAC-8 | 1800 | 1237 | 1.48 | 6.6 | 12 | 0.55 |
| TSAC-10 | 2520 | 1521 | 1.68 | 11.1 | 23 | 0.48 |
| TSWAC-8 | 5240 | 1920 | 2.73 | 19.25 | 39 | 0.49 |
| TSWAC-10 | 6140 | 2769 | 2.22 | 30.3 | 55 | 0.55 |

**Table 5 Failure modes and measures of ductility**

| Specimen | Predicted failure mode | Actual failure mode | maximum recorded rotation Φc (mrad) | $M_{j,max}/M_{j,R}$ |
|---|---|---|---|---|
| FEP | End plate in bending | Fracture of bolt in tension | 165 | 1.63 |
| EEP | End plate in bending | Bolt failure in tension | 121 | 1.91 |
| TSAC-8 | Bending of flange cleat/mode1 | Bolt failure in tension and shear | 157 | 2.83 |
| TSAC-10 | Bending of flange cleat/mode 1 | Bolt failure in tension and shear | 162 | 1.80 |
| TSWAC-8 | Bending of flange/mode 1-bending of web cleat /mode 1 | Bolt failure in tension and shear (flange cleat bolt) | 131 | 1.88 |
| TSWAC-10 | Bending of flange/mode 1-bending of web cleat /mode 1 | Bolt failure in shear (top bolt connecting web cleat to beam web) | 95 | 1.36 |